Biomedical Optics EXPRESS

Hollow core photonic crystal fiber for monitoring leukemia cells using surface enhanced Raman scattering (SERS)

Altaf Khetani,[1,*] Ali Momenpour,[1] Emilio I. Alarcon,[2] and Hanan Anis[1]

[1]*School of Electrical Engineering and Computer Science (EECS), University of Ottawa, Ottawa, ON K1N 6N5, Canada*

[2]*University of Ottawa Heart Institute, Division of Cardiac Surgery Research, 40 Ruskin Street, Ottawa, ON K1Y 4W7 Canada*

[*]*akhet035@uottawa.ca*

Abstract: The present paper demonstrates an antibody-free, robust, fast, and portable platform for detection of leukemia cells using Raman spectroscopy with a 785-nm laser diode coupled to a hollow core photonic crystal (HC-PCF) containing silver nanoparticles. Acute myeloid leukemia is one of the most common bone marrow cancers in children and youths. Clinical studies suggest that early diagnosis and remission evaluation of myoblasts in the bone marrow are pivotal for improving patient survival. However, the current protocols for leukemic cells detection involve the use of expensive antibodies and flow cytometers. Thus, we have developed a new technology for detection of leukemia cells up to 300 cells/ml using a compact fiber HC-PCF, which offers a novel alternative to existing clinical standards. Furthermore, we were also able to accurately distinguish live, apoptotic and necrotic leukemic cells.

OCIS codes: (280.4788) Optical sensing and sensors; (060.5295) Photonic crystal fibers; (170.5660) Raman spectroscopy; (170.1530) Cell analysis; (240.6695) Surface-enhanced Raman scattering.

References and links

1. D. K. Graham, D. B. Salzberg, J. Kurtzberg, S. Sather, G. K. Matsushima, A. K. Keating, X. Liang, M. A. Lovell, S. A. Williams, T. L. Dawson, M. J. Schell, A. A. Anwar, H. R. Snodgrass, and H. S. Earp, "Ectopic expression of the proto-oncogene Mer in pediatric T-cell acute lymphoblastic leukemia," Clin. Cancer Res. **12**(9), 2662–2669 (2006).
2. K. Zhang, T. Tan, J. J. Fu, T. Zheng, and J. J. Zhu, "A novel aptamer-based competition strategy for ultrasensitive electrochemical detection of leukemia cells," Analyst (Lond.) **138**(21), 6323–6330 (2013).
3. C. M. Brown, S. R. Larsen, H. J. Iland, D. E. Joshua, and J. Gibson, "Leukaemias into the 21st century: part 1: the acute leukaemias," Intern. Med. J. **42**(11), 1179–1186 (2012).
4. Z. Darzynkiewicz, and H. Zhao, *Cell cycle analysis by flow cytometry* eLS (2014).
5. H. G. Goh, M. Lin, T. Fukushima, G. Saglio, D. Kim, S. Y. Choi, S. H. Kim, J. Lee, Y. S. Lee, S. M. Oh, and D. W. Kim, "Sensitive quantitation of minimal residual disease in chronic myeloid leukemia using nanofluidic digital polymerase chain reaction assay," Leuk. Lymphoma **52**(5), 896–904 (2011).
6. R. J. Olsen, C. C. Chang, J. L. Herrick, Y. Zu, and A. Ehsan, "Acute leukemia immunohistochemistry: a systematic diagnostic approach," Arch. Pathol. Lab. Med. **132**(3), 462–475 (2008).
7. C. Righeschi, T. Eichhorn, A. Karioti, A. R. Bilia, and T. Efferth, "Microarray-based mRNA expression profiling of leukemia cells treated with the flavonoid, casticin," Cancer Genomics Proteomics **9**(3), 143–151 (2012).
8. R. Li, Y. Tan, X. Chen, F. Ren, Y. Zhang, Z. Xu, and H. Wang, "Fluorescence probe analysis of leukemia cells by modified graphene oxide," Carbon **85**, 446 (2015).
9. R. McCreery, *Raman Spectroscopy for Chemical Analysis* (New York: John Wiley and Sons, 2000).
10. J. Ferraro, K. Nakamoto, and C. Brown, *Introductory Raman Spectroscopy*, 2nd ed. (Elsevier 2003).
11. M. Buric, *Gas phase Raman spectroscopy using hollow waveguides*, (Thesis Diss. University of Pittsburgh, 2011).
12. R. Altkorn, I. Koev, R. P. Van Duyne, and M. Litorja, "Low-loss liquid-core optical fiber for low-refractive-index liquids: fabrication, characterization, and application in Raman spectroscopy," Appl. Opt. **36**(34), 8992–8998 (1997).

#247759 Received 11 Aug 2015; revised 18 Sep 2015; accepted 21 Sep 2015; published 28 Oct 2015

13. M. Holtz, P. Dasgupta, and G. Zhang, "Small-volume raman spectroscopy with a liquid core waveguide," Anal. Chem. **71**(14), 2934–2938 (1999).
14. X. M. Qian and S. M. Nie, "Single-molecule and single-nanoparticle SERS: from fundamental mechanisms to biomedical applications," Chem. Soc. Rev. **37**(5), 912–920 (2008).
15. Y. J. Oh, S. G. Park, M. H. Kang, J. H. Choi, Y. Nam, and K. H. Jeong, "Beyond the SERS: Raman enhancement of small molecules using nanofluidic channels with localized surface plasmon resonance," Small **7**(2), 184–188 (2011).
16. C. W. Freudiger, W. Min, B. G. Saar, S. Lu, G. R. Holtom, C. He, J. C. Tsai, J. X. Kang, and X. S. Xie, "Label-free biomedical imaging with high sensitivity by stimulated Raman scattering microscopy," Science **322**(5909), 1857–1861 (2008).
17. P. Russell, "Photonic-crystal fibers," J. Lightwave Technol. **24**(12), 4729–4749 (2006).
18. A. Campion and P. Kambhampati, "Surface-enhanced Raman scattering," Chem. Soc. Rev. **27**(4), 241–250 (1998).
19. A. Khetani, A. Momenpour, V. Tiwari, and H. Anis, *Surface Enhanced Raman Scattering (SERS) using Nanoparticles* (Springer International Publishing, 2015).
20. H. Yan, C. Gu, C. Yang, J. Liu, G. Jin, J. Zhang, L. Hou, and Y. Yao, "Hollow core photonic crystal fiber surface-enhanced Raman probe," Appl. Phys. Lett. **89**, 204101 (2006).
21. V. S. Tiwari, A. Khetani, M. Naji, and H. Anis, "Study of Surface Enhanced Raman Scattering (SERS) within hollow core photonic crystal fiber," IEEE Sensors **5404**, 367–370 (2009).
22. V. S. Tiwari, A. Khetani, A. Momenpour, and H. Anis, "Optimum size and volume of nano particles within hollow core photonic crystal fiber," IEEE J. Quantum Electron. **20**, 7300608 (2014).
23. T. Shimizu and Y. Pommier, "Camptothecin-induced apoptosis in p53-null human leukemia HL60 cells and their isolated nuclei: effects of the protease inhibitors Z-VAD-fmk and dichloroisocoumarin suggest an involvement of both caspases and serine proteases," Leukemia **11**(8), 1238–1244 (1997).
24. M. Gupta, A. Fujimori, and Y. Pommier, "Eukaryotic DNA topoisomerases I," BBA-Gene Struct. Expr. **1262**, 1–14 (1995).
25. Y. Pommier, "Eukaryotic DNA topoisomerase I: genome gatekeeper and its intruders, camptothecins," Semin. Oncol. **23**(1 Suppl 3), 3–10 (1996).
26. N. Leopold and B. Lendl, "A new method for fast preparation of highly surface-enhanced Raman scattering (SERS) active silver colloids at room temperature by reduction of silver nitrate with hydroxylamine hydrochloride," J. Phys. Chem. B **107**(24), 5723–5727 (2003).
27. A. Khetani, J. Riordon, V. Tiwari, A. Momenpour, M. Godin, and H. Anis, "Hollow core photonic crystal fiber as a reusable Raman biosensor," Opt. Express **21**(10), 12340–12350 (2013).
28. Y. Oshima, H. Shinzawa, T. Takenaka, C. Furihata, and H. Sato, "Discrimination analysis of human lung cancer cells associated with histological type and malignancy using Raman spectroscopy," J. Biomed. Opt. **15**(1), 017009 (2010).

1. Introduction

Acute myeloid leukemia (AML) is among the most recurrent pediatric cancers and remains the leading cause of disease-related morbidity in children and adolescents [1,2]. AML results in the abnormal production of blast cells in the bone marrow failure: if not treated, AML rapidly progresses within weeks, suppressing the normal production of platelets and white blood cells, and leading to life threatening bleeding and microbial infections. Hence, the early detection of AML [3] as well as evaluation of minimal residual disease (MRD) after treatment completion, positively improves the patient's life expectancy. The current standard techniques that include flow cytometry [4], polymerase chain reaction [5], immunohistochemistry [6], microarray [7], and fluorescence-based assays [8], are relatively difficult/costly to implement and time-consuming. Consequently, it is still a major challenge to develop new more affordable and fast technologies for AML detection.

Raman spectroscopy is an analytical, non-destructive technique that provides information about the molecular structure of the investigated sample [9]. The Raman effect arises when an incident light illuminates molecules, which subsequently scatter light. While most of this scattered light is at the same wavelength as the incident light, a fraction of that scattered is at a different wavelength. A key limitation of the Raman effect is its extremely weak signal (*i.e.*, 1 in million photon actually exhibits the change in wavelength), which means that high-power lasers and longer acquisition times are required [10]. However, high laser power can damage samples and limits the biological uses of Raman spectroscopy. Fortunately, there are other ways to increase a weak Raman signal, including (i) hollow core waveguides [11–13], (ii)

#247759 Received 11 Aug 2015; revised 18 Sep 2015; accepted 21 Sep 2015; published 28 Oct 2015

surface-enhanced Raman scattering (SERS) [14,15], and (iii) stimulated Raman scattering (SRS) [16].

A hollow-core waveguide supporting a single transverse mode with low attenuation losses and long interaction length possess the right attributes for enhancing a Raman signal. The hollow core photonic crystal fiber (HC-PCF) is a novel type of optical waveguide that allows the target sample to be infiltrated into the hollow core and cladding [17]. HC-PCF provide prolonged interaction length with very low losses compared to conventional cuvette geometry, achieving high spatial confinement of the target molecules. The light guidance in HC-PCF occurs via a photonic band gap, which enables strong light-matter interaction and enhancement of the Raman signal.

One can further improve the sensitivity of HC-PCF-based Raman sensors by incorporating metal nanoparticles inside the HC-PCF fibers, leading to surface enhanced Raman scattering (SERS). SERS is a powerful analytical method for the detection and identification of extremely low concentrations of molecular species [18]. It overcomes the low Raman cross-section barrier by exploiting the large field enhancement due to electromagnetic coupling between the nanoparticles [19]. Under such conditions, the Raman signal of the target molecule is enhanced by several orders of magnitude, enabling detection down to single molecule scale. While HC-PCF offers higher interaction length between the light and the analyte and lower sample consumption, SERS provides large enhancement factors to increase the sensitivity of normal Raman signal, thereby enabling detection of molecules in various applications. Thus, the integration of HC-PCF and SERS provides an ideal platform for detection of biomolecules [20, 21].

In our previous work, we have reported a detection scheme that exploits Raman spectroscopy to determine the optimal volume and size of silver nanoparticles to maximize the Raman signal enhancement of rhodamine 6G (R6G) within HC-PCF [22]. In this paper, we have integrated HC-PCF with nanoparticles to form a portable sensor that detects malignant cells, such as HL60 acute myeloid leukemia. The main advantage of the proposed sensor is the possibility of rapid analysis and diagnosis. The organization of the paper is as follows: we begin with a brief description about HC-PCF and present a layout of the Raman setup. This is followed by nanoparticle synthesis and cell culture. Successive sections summarize our findings on the enhancement in Raman signal from leukemia samples, distinguishing apoptotic, live and necrosis cell cycle stages. The last section presents the Raman sensor detection limit with respect to flow cytometry.

2. Experimental

2.1 Theory of HC-PCF

The light guiding property of non-selectively filled HC-PCFs depends on the refractive index of the filled sample. In this case, the guiding principle is still due to bandgap effect, but the transmission band supported by the fiber is shifted. The details of choosing the fiber depends on the wavelength and refractive index of liquid sample and can be found in our previous work [22]. In our case, 785-nm was chosen to be the excitation wavelength and hence, an HC-1550 hollow core photonic bandgap fiber from NKT Photonics was initially chosen. The fiber has a core size of 10.6μm (± 1μm) supporting the center wavelength 1550 nm with a bandwidth of ~200nm. Since leukemia cells are >10μm in diameter, HC19-1550 is a variant of HC-1550 fiber formed by removing 19 cells from the cladding of the fiber so that core diameter becomes 20μm. HC19-1550 has a core size of 20μm (± 2μm) supporting 1570nm center wavelength with bandwidth of 100nm. Figure 1 shows a cross-section view of HC19-1550 fiber and the mode-field pattern of the filled HC-PCF fiber with leukemia cells and nanoparticles. The modal field diameter was found to be ~4.5mm as shown in Fig. 1(b); that is quite close to the theoretically calculated value of 4.2mm. We found similar mode field pattern for other sets of sample solutions with different leukemia cell cycle stages and

#247759 Received 11 Aug 2015; revised 18 Sep 2015; accepted 21 Sep 2015; published 28 Oct 2015

different concentrations of leukemia cells. Thus, it was confirmed that propagation properties did not change appreciably with the different leukemia samples.

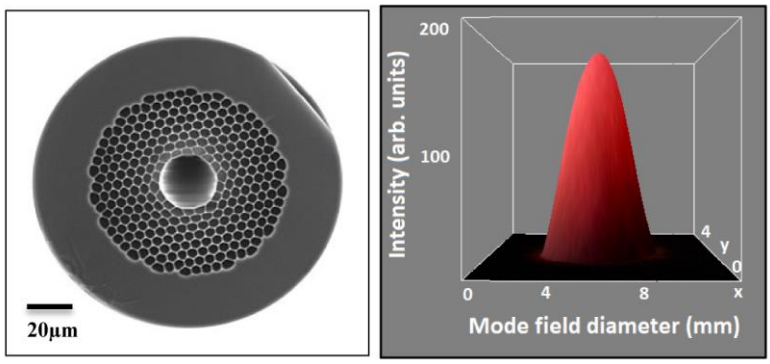

Fig. 1. Hollow core photonic crystal fiber HC19-1550 (a) SEM image courtesy NKT Photonics Inc. (b) spatial distribution of modal field of leukemia sample solution filled HC-PCF imaged using a CCD camera (Canon) exhibiting a perfect Gaussian profile.

2.2 Sample preparation

Acute promyelocytic leukemia (HL60) cells (ATCC® CCL-240) were cultured in Iscove's Modified Dulbecco's Medium (Sigma), supplemented with 20% fetal bovine serum and 1% antibiotics (streptomycin and penicillin) and 0.1% gentamicin. Cells were incubated at 37°C, 5.0% CO_2 and 100% humidity. In all cases, cell density was kept between 0.1 and $1.0x10^6$ cells/ml. Apoptosis was induced by incubating the cells with 5.0 µM (*S*)-(+)-Camptothecin (CPT), a topoisomerase I inhibitor [23–25] for three hours in Hanks Buffer (Sigma) using a $1x10^5$ cells/ml density. Then, the cells were centrifuged at 1000 rpm for 5 min and the pellet was resuspended in 100 µL ($1x10^6$ cells/ml cell density) of Annexin binding buffer (Life Technologies) and 1.0 µL of 50 µg/mL propidium iodide (PI) and 5.0 µL Annexin V-FITC added to the cells. The mixture was incubated at room temperature for 15 minutes and then another 400 µL of Annexin buffer added to the mixture prior sorting in a BD FACS-Aria flow cytometer. Cell sorting was carried out by gating no stained cells (live), PI and annexin V positive staining (necrotic; λ_{exc} = 488 nm, λ_{em} = 585 ± 21 nm), and Annexin V positive (apoptotic λ_{exc} = 488 nm, λ_{em} = 530 ± 15 nm). Cell number in all cases were measured in a Vi-Cell (Beckman Coulter). Additional experiments were carried out for non-stained cells following the scattering profile in the flow cytometer. In those experiments, the total number of cells was varied between 25,000 and 310 cells/mL using serial dilution in the cell culture medium without phenol red. Control experiments were also carried out following the same dilution procedure of the cell culture medium without cells.

Nanoparticles Synthesis: The role of nanoparticles is to enhance the weak Raman signal of molecules/cells which is correlated with their concentrations. Silver nanoparticles were prepared by chemical reduction in an aqueous solution of silver nitrate, according to the method described by Leopold *et al*. [26] which is as follows: A 4.5 mL of sodium hydroxide solution (0.1 M) was added to 5 mL of hydroxylamine hydrochloride solution (0.06 M). The mixture was added rapidly to 90 mL of silver nitrate solution (0.001 M) and shaken for a few seconds producing a milky gray color solution. The nanoparticles were used within 2 hours of preparation. The UV–vis absorption spectrum and TEM images of AgNP are shown in Fig. 2. Silver spheres show only one principal plasmon band ~430 nm and the majority of silver nanoparticles were sphericalwith average size ~60nm.

#247759 Received 11 Aug 2015; revised 18 Sep 2015; accepted 21 Sep 2015; published 28 Oct 2015

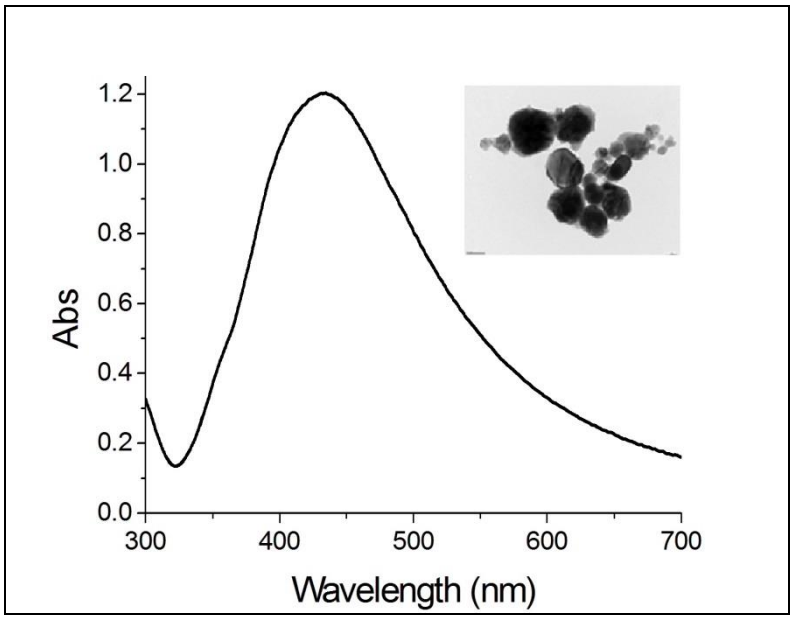

Fig. 2. UV-Vis absorption spectrum of silver nanoparticles. Inset shows the TEM image of spherical silver nanoparticles of ~60nm size.

2.3 Experimental configuration

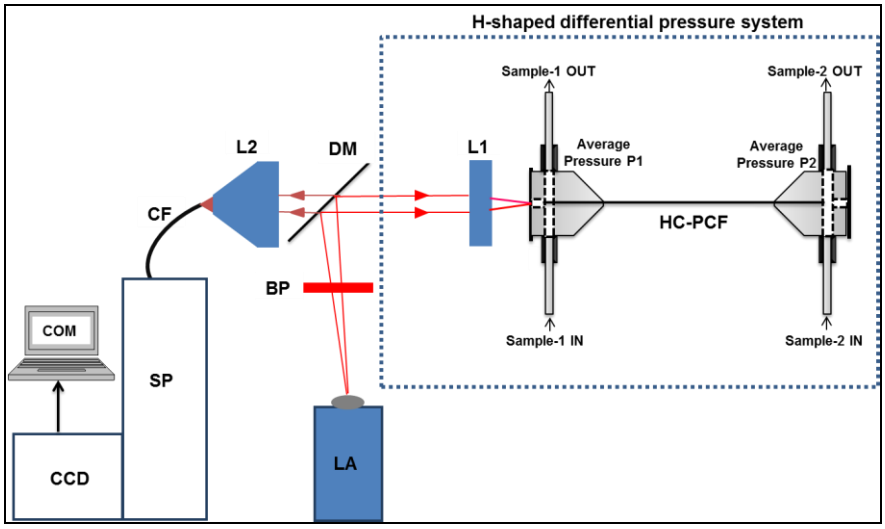

Fig. 3. Schematic of the setup. LA: Laser source with collimating lens; BP: Band pass filter; DM: Dichroic Mirror; L1: Microscope objective lens for light coupling; H-shaped differential pressure system with hollow core photonic crystal fiber; L2: Microscope objective lens for backward light collection; CF: Collection fiber; SP: spectrograph; CCD: CCD camera; COM: Computer.

The layout of the HC-PCF sensor is shown in Fig. 3. It consists of two segments-optics and Hshaped differential pressure system. The optical assembly employed a single mode 100-mW, 14-pin butterfly pin laser (Photonic Solutions) with a central wavelength of 785 nm. The laser beam was passed through a bandpass filter (BP) centered at 785-nm (± 2.0 nm) to filter out other wavelength components around 785-nm from the laser diode. Then, it was directed through a dichroic filter (R785RDC, Chroma Technologies Corp.) which reflected 785-nm (±

#247759 Received 11 Aug 2015; revised 18 Sep 2015; accepted 21 Sep 2015; published 28 Oct 2015

5.0 nm) at an angle of 45° and transmitted the 790-1000 nm band. The dichroic filter acted as a reflector for the laser beam which was further focused onto the tip of the HC-PCF by a 40x microscopic objective lens (L1) with numerical aperture (N.A) of ~0.65. The light coupling efficiency for leukemia and nanoparticles solution filled in HC-PCF was ~30%. Furthermore, the dichroic filter acted as a high pass filter for the light scattered backward from the sample-filled HC-PCF, thus allowing only the Raman wavelength to pass through it. The filtered Raman light was then imaged onto a fiber bundle (Fiberoptic System Inc., 26 multimode fiber, NA = 0.22) by another 6.3x microscopic objective lens (L2) with N.A as ~0.22. The output of the fiber bundle was connected to a Kaiser f/1.8i Spectrograph with a TE-cooled Andor CCD camera. The Andor SOLIS software was used for spectral data acquisition and spectra were monitored on the data acquisition computer.

The other segment of sensor configuration is comprised of two parallel channels (tubing)-one for sample (leukemia cells) input/output and the other for purging fluid (water) input/output. The integration of HC-PCF perpendicularly with the two parallel fluidic channels looks like an H-shaped structure as shown in the Fig. 3. In order to flow sample 1 (sample mixture) inside the fiber channels, average pressure P1 was kept higher than the average pressure P2. This ensured the liquid can be filled. Similarly, for purging out sample from HC-PCF fiber, the pressure was reversed, i.e., average pressure P2 was kept higher than the average pressure P1. The average pressure and the rate at which the sample is pumped into the fiber is discussed in detail [27].

3. Results and discussion

3.1 Enhancement of Raman signal with HC-PCF and nanoparticles

The first part of our investigation focused on recording Raman spectra from HL60 cells with $1x10^6$ cells/ml in cuvette and mixture of nanoparticle in HC-PCF. The Raman spectra of leukemia cells in cuvette is shown in Fig. 4, which has peaks at 1032 cm^{-1}(C-N stretching mode of phenylalanine) and 1318 cm^{-1} (protein). The mixture of leukemia cells and nanoparticles in HC-PCF produced a rich spectrum with obvious features around 650 cm^{-1} (protein:C-S stretching, tryptophan: C-N stretching), 722 cm^{-1} (C-H rocking of CH_2 methylene group in lipids), 789 cm^{-1} (O-P-O ring breathing modes of DNA/RNA bases), 1003 cm^{-1} (symmetric ring breathing mode of phenylalanine), 1032 cm^{-1} (C-N stretching mode of phenylalanine), 1093 cm^{-1} (O-P-O symmetric stretching mode of protein), 1119 cm^{-1} (C-N stretching mode of protein), 1283 cm^{-1} (amide III), 1318 cm^{-1} (protein), 1436 cm^{-1} (C-H bending of lipids) [2, 28]. In this experiment our aim was to determine the factor by which HC-PCF and nanoparticles enhance the Raman signal, which we found to be ~2,700. The HC-PCFs are known to enhance the Raman signal as it supports strong modal field overlap with the sample due to its photonic band gap property. The enhancement factor of the sensor was calculated by dividing the Raman signal of leukemia cells and nanoparticles from HC-PCF by the Raman signal of leukemia cells from the cuvette.

#247759 Received 11 Aug 2015; revised 18 Sep 2015; accepted 21 Sep 2015; published 28 Oct 2015

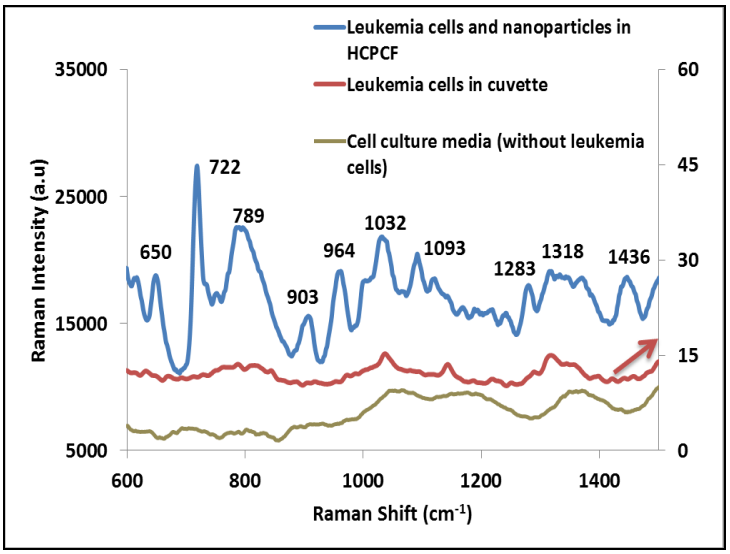

Fig. 4. Enhancement of Raman signal of HL60 cells in HC-PCF using silver nanoparticles.

3.2 Multivariate analysis

In the next phase of our demonstration, we have used statistical analysis for distinguishing the cell cycle states. Principal component analysis (PCA) and partial least squares (PLS) are very important parts of multivariate data analysis and have the main role to verify and detect classification and minimum level of different leukemia cells. The Unscrambler version 10.3 (CAMO, Corvallis, OR, USA) was used to perform the multivariate data analysis. In PCA analysis, variations in the data set are used for their identification and interpretation. The projection of X-variable (spectral wavelength) and Y-variable (analytical data) to a new space of so-called principal components (PCs) is the basis of PCA. The first PC is defined as the direction of the most variations in Y-variable, the second PC, which is orthogonal to the first PC, is defined as the direction of the second most variance (that not described by the first PC), and so on. Scores show the similarities or differences among samples. Similar samples have close scores along the same PC. The plotting of any PCs against each other could be used to interpret the structure of observations and reveal the hidden structure of spectra. The score plot of PC1 and PC2 is shown in Fig. 5 and discloses different groups in the samples. The PCA analysis on the different cycle stages of live, necrotic, and apoptotic HL60 cells yields a distinct Raman signature which is clearly distinguishable.

#247759 Received 11 Aug 2015; revised 18 Sep 2015; accepted 21 Sep 2015; published 28 Oct 2015

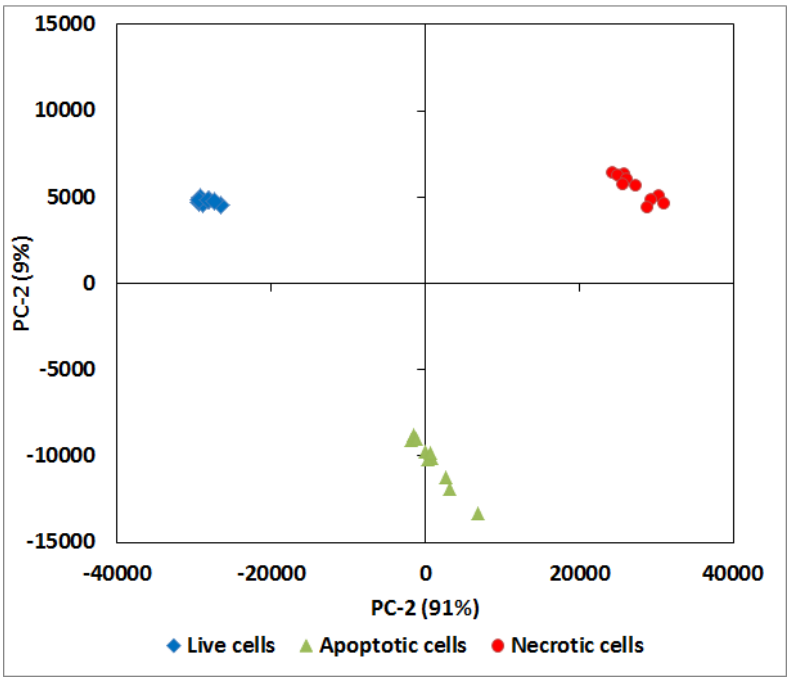

Fig. 5. Plots of principal component analysis (PCA) analysis of Raman spectra of different leukemia cells stages showing distinguishable live, apoptotic and necrotic cell stages.

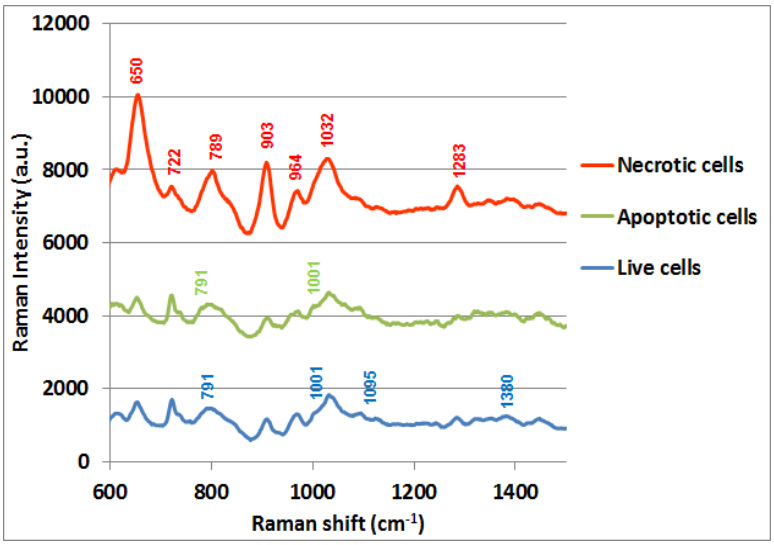

Fig. 6. Raman spectra of leukemia cells cycle stages with distinguishing Raman peaks in live, apoptotic and necrotic cells.

Raman spectra of different cells cycle stages are shown in Fig. 6 and indicate the variation of Raman intensity at important wavenumbers. Most of the necrotic Raman bands show higher intensity than live and apoptotic cells except at 722 cm^{-1} and 1001 cm^{-1}. Also the average of intensity of bands in apoptotic cells is higher than for live cells. These spectra along with score plot of PCA enable us to distinguish these cells from each other.

#247759 Received 11 Aug 2015; revised 18 Sep 2015; accepted 21 Sep 2015; published 28 Oct 2015

3.3 SERS in HC-PCF for different Leukemia cells concentrations

In the next part of our investigation, we recorded Raman spectra of different concentrations of leukemia cells and nanoparticles in HC-PCF. Figure 7 shows SERS spectra at six different concentrations of leukemia cells. As discussed earlier, Raman peaks at 650 cm^{-1} (protein:C-S stretching, tryptophan: C-N stretching), 722 cm^{-1} (C-H rocking of CH_2 methylene group in lipids), 789 cm^{-1} (O-P-O ring breathing modes of DNA/RNA bases), 1003 cm^{-1} (symmetric ring breathing mode of phenylalanine), 1032 cm^{-1} (C-N stretching mode of phenylalanine), 1093 cm^{-1} (O-P-O symmetric stretching mode of protein), 1119 cm^{-1} (C-N stretching mode of protein), 1318 cm^{-1} (protein), and 1436 cm^{-1} (C-H bending of lipids) were the prominent peaks from different concentrations of the samples. Once we recorded the Raman spectra of different concentrations of HL60 cells, we applied multivariate analysis for correlating Raman signal with sample concentrations.

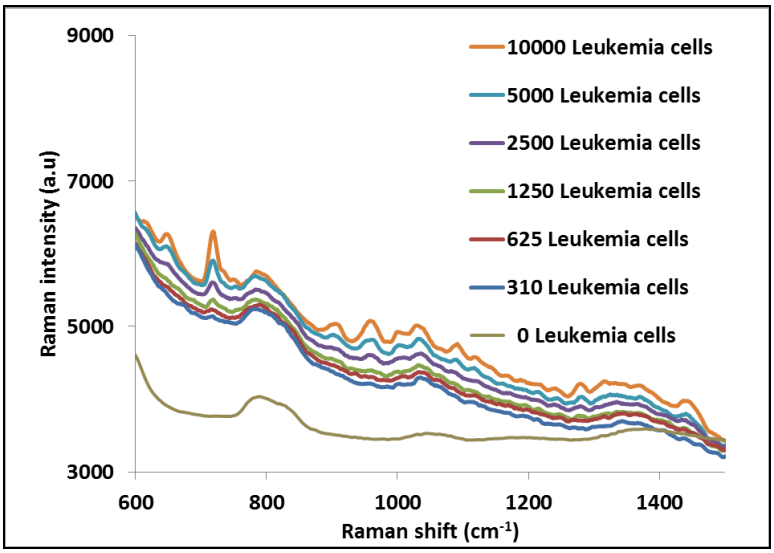

Fig. 7. SERS spectra of different concentrations of live HL60 cells, expressed as cells/ml.

In PLS analysis, the spectral data are used to generate a calibration model. This model is used to predict the dependent variables, such as analyte concentrations, by using the spectral response of the analyte. The validation of PLS model is also an essential requisite of data processing which verifies the generated model. Full cross validation (FCV) and test set validation (TSV) are two different methods which can be used to validate a model. In FCV, one spectral data set is left out for validation while the rest of the spectral data sets are used for developing the calibration model. This validation process (FCV) is then repeated for each sample in the entire data set. In TSV, the spectral data is split into two parts. One part contains the spectral data used to make a model and the other part which contains the rest of spectral data to fit into the model and compare the computed value with the observed value for those samples.

#247759 Received 11 Aug 2015; revised 18 Sep 2015; accepted 21 Sep 2015; published 28 Oct 2015

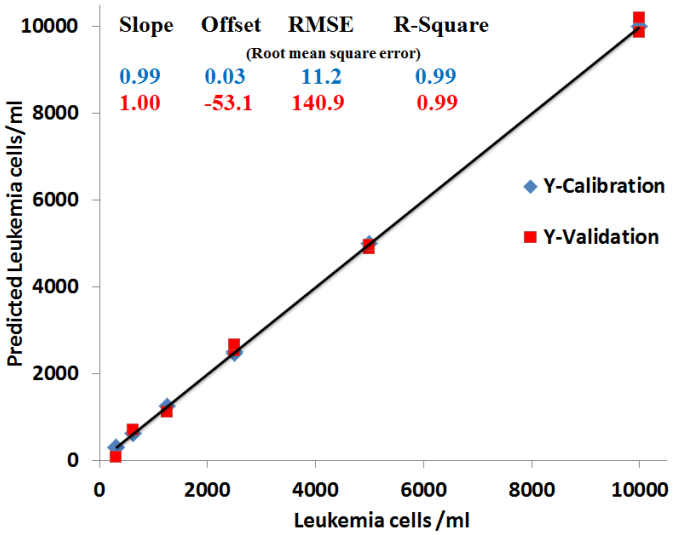

Fig. 8. PLS prediction of different concentrations of leukemia cells/ml showing excellent correlation between calibrated and predicted samples with $R^2 = 0.99$ and RMSEC and RMSEP of 11 and 140 cells/ml.

The performance of a model can be expressed in terms of statistical parameters, including root mean square error of calibration (RMSEC), root mean square error of prediction (RMSEP), and coefficient of determination (R^2). The Raman spectra of six samples were recorded. To ensure repeatability of measurement, for each sample, 10 Raman spectra were recorded. The Raman spectra of six samples were splitted into 3 subsets; calibration set, validation set, and test set. The calibration and validation sets were used to make the model while the test set as an independent data was used to evaluate the model. Three of the recorded spectra were identified as outliers and were not used for making the model by the Unscrambler software. According to the PLS model of 45 records of samples, which were in calibration and validation sets, R^2 (for calibration and validation) RMSEC, and RMSEP are 0.99, 0.99, 11, and 140, respectively. The calibration curve of this model is shown in Fig. 8.

3.4 Comparing HC-PCF sensor with flow cytometry

Flow cytometry experiments using non-stained cells were also carried out to compare this technique with our HC-PCF method. The data shown in Fig. 9 clearly shows the lack of linearity between the number of events detected by the systems with the total number of cells in the solution. In fact, we had found that the lower limit of detection, compared to solutions without cells, was found to be between 500 and 2500 cells/mL. Figure 9 inset shows the red region which denotes the 500 cells/ml limit we consistently found as background under our experimental conditions, see right panels in Fig. 9. In addition, this inset also shows how the point at 2500 cells/mL does not correlate with the total number of events detected for the equipment. Furthermore, from a simple visual inspection of Fig. 9, it can be seen an upward curvature which again indicates the poor correlation between the actual number of cells in the sample and those detected by the system.

#247759 Received 11 Aug 2015; revised 18 Sep 2015; accepted 21 Sep 2015; published 28 Oct 2015

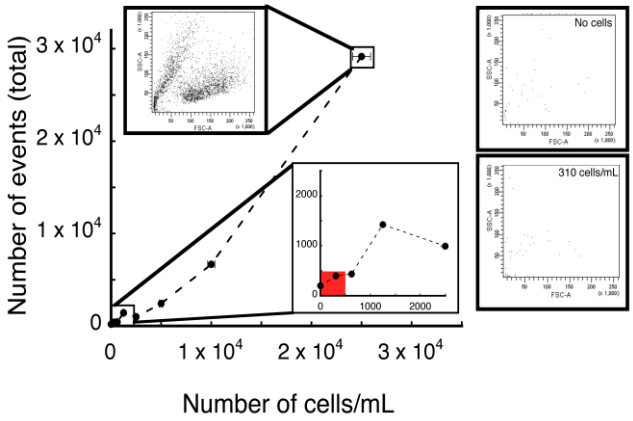

Fig. 9. Number of events vs. total number of cells/mL for HL60 cells. Number of events was quantified by using the scattering upon 488-nm excitation of a non-stained cell suspension. Top inset shows the scattering profile for the sample containing 25,000 cells/mL. Bottom inset shows a magnification for the lower cell numbers where the red area denotes the noise region or lower limit of detection for the system. Right panels include the scattering profile for the sample with 310 cells/mL and a control solution without any cells, where it can be clearly seen the close similarity between the two plots.

4. Conclusions

We have demonstrated a robust and sensitive platform for monitoring and detecting leukemia cells. The present scheme uses nanoparticles and hollow core photonic crystal fiber for enhancing the weak Raman signal of leukemia cells. We have obtained an enhancement of ~2700 using this scheme. In addition, we have applied PCA statistical analysis for differentiating apoptotic, live and necrotic cells. We have also applied PCA analysis on different cell count demonstrating the capability of the sensor to detect lower cell counts. For our sensor, we were successfully able to detect ~300 cells/ml.

Acknowledgement

This work was supported by NSERC Discovery and University of Ottawa Heart Institute. The authors would like to thank Mrs. Suzanne Crowe for her assistance in the flow cytometry experiments.